Available online at www.sciencedirect.com

ScienceDirect

Rice Science, 2024, 31( ): −

Research Paper

Potential Secretory Transporters and Biosynthetic Precursors of Biological Nitrification Inhibitor 1,9-Decanediol in Rice as Revealed by Transcriptome and Metabolome Analyses

DI Dongwei[1], MA Mingkun[1, 4], ZHANG Xiaoyang[1], LU Yufang[1], Herbert J. KRONZUCKER[3], SHI Weiming[1, 2, 4]

([1]*State Key Laboratory of Soil and Sustainable Agriculture, Institute of Soil Science, Chinese Academy of Sciences, Nanjing 210008, China;* [2]*School of Food Science and Engineering, Foshan University, Foshan 528000, China;* [3]*School of BioSciences, The University of Melbourne, Parkville, VIC 3010, Australia;* [4]*University of Chinese Academy of Sciences, Beijing 100049, China*)

Abstract: Biological nitrification inhibitors (BNIs) are released from plant roots and inhibit the nitrification activity of microorganisms in soils, reducing NO_3^- leaching and N_2O emissions, and increasing nitrogen-use efficiency (NUE). Several recent studies have focused on the identification of new BNIs, while little is known about the genetic loci governing their biosynthesis and secretion. We applied a combined transcriptomic and metabolomic analysis to investigate possible biosynthetic pathways and transporters implicated in the biosynthesis and release of BNI 1,9-decanediol (1,9-D), previously identified in rice root exudates. Our results link four fatty acids, icosapentaenoic acid, linoleate, norlinolenic acid, and polyhydroxy-α,ω-divarboxylic acid, to 1,9-D biosynthesis, and three transporter families, namely the ATP-binding cassette protein family, the multidrug and toxic compound extrusion family, and the major facilitator superfamily, to 1,9-D release from roots into the soil medium. Our results provide candidates for further work on the genes implicated in the biosynthesis and secretion of 1,9-D and pinpoint genetic loci for crop breeding to improve NUE by enhancing 1,9-D secretion, with the promise of reducing NO_3^- leaching and N_2O emissions from agricultural soils.

Key Words: biological nitrification inhibitor; nitrogen-use efficiency; 1,9-decanediol; transcriptomic analysis; metabolomic analysis

The two main sources of nitrogen (N) utilized by higher plants are ammonium-N (NH_4^+) and nitrate-N (NO_3^-). NH_4^+ can be readily converted to NO_3^- through the process of nitrification, carried out by soil microorganisms, but the extent to which conversion takes place varies greatly among soil environments (Kronzucker et al, 1997; Kronzucker et al, 1999; Kaur-Bhambra et al, 2022). Unlike the cationic NH_4^+ form, which is retained well in most soil types, the anionic NO_3^- form can leach from soils into water systems and cause environmental pollution, while denitrification produces various gaseous forms of N, including N_2O, NO and N_2, of which N_2O is a potent greenhouse gas and, thus, resulting in global warming (Coskun et al, 2017b; Min and Shi 2018; Min et al, 2021; Souza et al, 2021; Li et al, 2022; Elrys et al, 2023). Nitrification inhibitors, including both synthetic nitrification inhibitors and biological nitrification inhibitors, inhibit nitrification carried out by soil bacteria and thereby reduce NO_3^- loss and N_2O emission and improve nitrogen-use efficiency (NUE) (Subbarao et al, 2013b, c; Coskun et al, 2017a, b). In contrast to the typically lower efficacy and higher environmental pollution potential of synthetic nitrification inhibitors, biological nitrification

Received: 1 June 2023; **Accepted:**

Corresponding author: SHI Weiming (wmshi@issas.ac.cn)

Peer review under responsibility of China National Rice Research Institute

http://dx.doi.org/

inhibitors (BNIs) released from plant roots possess high efficacy and are more environmentally friendly (Subbarao et al, 2015; Woodward et al, 2016).

In the past two decades, several BNIs, including methyl 3-(4-hydroxyphenyl) propionate (MHPP), sakuranetin, sorgoleone, brachialactone, syringic acid, 2,7-dimethoxy-1,4-naphthoquinone, 2-hydroxy-4,7-dimethoxy-2H-1,4-benzoxazin-3(4H)-one, 6-methoxy-2(3H)-benzoxazolone, oxalic acid and protocatechuic aldehyde, have been identified from *Sorghum bicolor*, *Brachiaria humidicola*, *Oryza sativa*, *Triticum aestivum*, *Leymus racemosus*, *Zea mays* and *Suaeda salsa* (Zakir et al, 2008; Subbarao et al, 2009, 2013a; Sun et al, 2016; Lu et al, 2022; Otaka et al, 2022; Wang et al, 2023). One practical approach of promoting NUE consists of rotating crops that can secrete BNIs from their roots with those that cannot or by mixing crude extracts from BNI-secreting plants with standard fertilizers (Wang et al, 2023). For example, rotations of sorghum and vegetables can effectively reduce N_2O emissions and increase NUE in vegetable crops, while *Moringa* extracts have been shown to simultaneously inhibit soil urease activity, soil nitrification and urea degradation, resulting in greatly improved NUE in potato tubers (Zhang et al, 2015; Elrys et al, 2019). The biosynthetic pathways of BNIs and their regulation are, in most cases, only scantily understood. Recently, Wang et al (2023) employed a multi-omic analysis to draw inferences about the biosynthetic pathways of protocatechuic aldehyde and oxalic acid in *S. salsa*. More generally, the identification of the pathways of BNI synthesis and targeting these by genetic engineering to improve BNI secretion or adding BNI-secretion capabilities to plants that cannot secrete BNIs would be a potent means to decrease NO_3^- leaching and N_2O emission from crop systems and to improve the NUE of crops (Subbarao et al, 2021).

Recently, we identified a new BNI from rice root exudates, 1,9-decanediol (1,9-D), a fatty alcohol compound that inhibits nitrification by blocking ammonia monooxygenase (AMO) in soil bacteria (Sun et al, 2016). A subsequent study showed that the release of 1,9-D from rice roots is stimulated by NH_4^+, pH modification and nitrifying bacteria (Zhang et al, 2019). A further study showed that 1,9-D inhibits nitrification through action on both ammonia-oxidizing bacteria and archaea in soil (Lu et al, 2019). In addition, our more recent study in *Arabidopsis* showed that 1,9-D promotes primary root growth by regulating abscisic acid content and PIN2-dependent auxin transport (Ma et al, 2023). Although past studies increased our understanding of 1,9-D, it remained unknown how 1,9-D is synthesized and how it is released from roots.

In recent years, multi-omic analysis has been used increasingly as an effective approach to identifying gene networks and regulatory pathways in a large variety of organisms (Fu et al, 2021; Wang et al, 2021). An integrated analysis of both the transcriptome and the metabolome has been deployed to uncover metabolic pathways in response to specific environmental and developmental signals (Cheng et al, 2022; Zhang Y T et al, 2022; Wang et al, 2023). In the present study, we used a combined transcriptome and metabolome analysis of two rice cultivars, Wuyunjing 7 (WYJ7, high 1,9-D release) and WYJ3 (no 1,9-D release), as well as NH_4^+-treated WYJ7, to identify the possible metabolic pathways involved in 1,9-D biosynthesis and to screen for possible genes encoding 1,9-D secretion carriers and/or channels by analyzing up-regulated genes related to transport carriers and/or channels in RNA-seq data. Our study sheds light on the genetic loci of 1,9-D synthesis and secretion and provides possible gene targets for screening rice varieties with high BNI secretion capacity, with the promise of reducing N losses from rice systems and improving NUE in this major crop species.

RESULTS

Rice varieties and rhizospheric NH_4^+ influence 1,9-D release

To identify key genes affecting the release of 1,9-D in rice, we performed a combined analysis of the transcriptome and metabolome. Our previous studies showed that N form (NH_4^+ or NO_3^-) and concentration, pH, aeration, bacterial inoculum (nitrifying or denitrifying bacteria) and rice variety all had an effect on 1,9-D release. Of these, NH_4^+ and varietal differences had a particularly pronounced effect on 1,9-D release (Sun et al, 2016; Zhang et al, 2019). In the current study, we first tested for 1,9-D release prior to transcriptomic and metabolomic analyses and, consistent with previous results, our results showed that external NH_4^+, supplied as NH_4Cl at 1 mmol/L, increased 1,9-D release in WYJ7 by 74%, while we did not detect any 1,9-D release in WYJ3 grown under control conditions, even after NH_4^+ treatment (Fig. 1). These clear differences in 1,9-D release between varieties and as a function of NH_4^+ treatment provided an excellent framework within which to explore transcriptomic and metabolomic analyses.

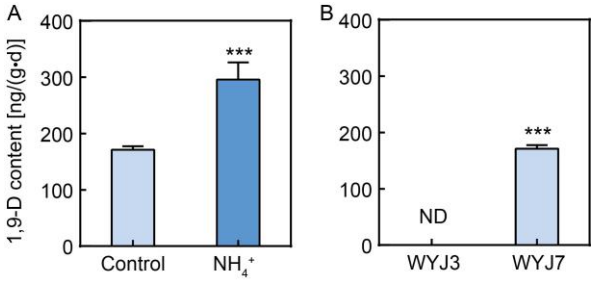

Fig. 1. Influence of NH_4^+ and variety on 1,9-decanediol (1,9-D) release in rice.

A, 1,9-D release from Wuyunjing 7 (WYJ7) roots with or without 1 mmol/L NH_4Cl treatment.

B, 1,9-D release in Wuyunjing 3 (WYJ3) and WYJ7 grown in control media.

Six-week-old seedlings were transferred to new solutions with 1 mmol/L $CaCl_2$ or 1 mmol/L NH_4Cl and grown for another 24 h prior to exudate collection. N.D. indicates not detected.

Data are Mean ±SD with four replications. ***, $P < 0.001$ (*t*-test).

Gas chromatography-mass spectrometer (GC-MS)-based metabolomics reveal distinct changes in metabolites in two experimental groups, $NH4^+$-WYJ7 vs CK-WYJ7 (N7/C7) and CK-WYJ7 vs CK-WYJ3 (C7/C3)

We first used GC-MS to identify differentially synthesized metabolites (DSMs) in N7/C7 and C7/C3.

Orthogonal partial least squares-discriminant analysis (OPLS-DA) divided all samples into different clusters, showing that variety and NH_4^+ treatment produced clear differences in metabolite accumulation (Fig. 2-A and -B). To prevent overfitting of the model, we further performed response permutation testing (RPT), and R2 values were 0.945 and 0.974 in N7/C7 and C7/C3, respectively, underscoring the reliability of the OPLS-DA models (Fig. S1). A single-dimensional analysis was used to screen DSMs in two groups, and 38 and 14 DSMs were identified in the N7/C7 and C7/C3 groups, respectively (Table S1; Fig. 2-C and -D). Of these DSMs, L-sorbose, 3-phosphoglyceric acid, D-mannose 6-phosphate, and galactinol were enriched more than 20-fold in WYJ7 after the NH_4^+ treatment, however, compared with C3, only two DSMs, vanillic acid and terephthalic acid, were up-regulated in C7 (Table S1). Subsequently, we further classified the DSMs by the Kyoto Encyclopedia of Genes and Genomes (KEGG) analysis. Compared with C3, the DSMs in C7 were significantly ($P < 0.05$) enriched in the ABC transporters, glutathione metabolism, and arginine biosynthesis, while the DSMs were significantly ($P < 0.05$) enriched in alanine, aspartate and glutamate metabolism, aminoacyl-tRNA biosynthesis, and glyoxylate and dicarboxylate metabolism in N7 compared with those in C7 (Fig. 2-D to -F and Table S2).

Liquid chromatograph-mass spectrometer (LC-MS)-based metabolomics reveal distinct changes in metabolites in two experimental groups, N7/C7 and C7/C3

To further examine the DSMs in different rice varieties and NH_4^+ treatment, we then analyzed the non-targeted metabolome of roots using LC-MS. We identified 735 and 508 DSMs ($P < 0.05$) in N7/C7 and C7/C3, respectively (Table S3). For these DSMs, OPLS-DA model analyses revealed distinct clusters between C7 and N7 and/or C3, indicating the existence of significantly different metabolites in the N7/C7 and C7/C3 groups (Fig. 3-A and -B). In the N7/C7 group, 481 up- and 254 down-regulated DSMs were obtained, which were enriched in 164 pathways, including 79 significant metabolic pathways ($P < 0.05$) (Fig. 3-C and –D; Table S4). The up-regulated DSMs were significantly enriched in linoleic acid metabolism, arachidonic acid metabolism, and glycerophospholipid metabolism, while the down-regulated DSMs were significantly enriched in citrate cycle (TCA cycle), histidine metabolism, and glyoxylate and dicarboxylate metabolism (Figs. 3-D and S5). Moreover, for the C7/C3 group, 43 up- and 465 down-regulated DSMs were identified and further classified into 52 metabolic pathways; of these, 27 pathways were significant ($P < 0.05$) (Fig. 3-E and -F; Table S4). For these DSMs in the C7/C3 group, up-regulated DSMs were significantly enriched in linoleic acid metabolism, arachidonic acid metabolism, and pantothenate and CoA biosynthesis, while down-regulated DSMs were significantly enriched in ABC transporters, glutathione metabolism, and galactose metabolism (Figs. 3-F and S3). Although there were differences in the metabolic pathways enriched in the N7/C7 and C7/C3 groups, the common up- or down-regulation of metabolic pathways also implies that the metabolic pathway responsible for 1,9-D biosynthesis in WYJ7 may be implicated in both the response to NH_4^+ and underpin the differences between rice varieties.

RNA-seq analysis reveals distinct changes in transcriptome in two experimental groups, N7/C7 and C7/C3

To obtain the potential genes involved in regulating 1,9-D

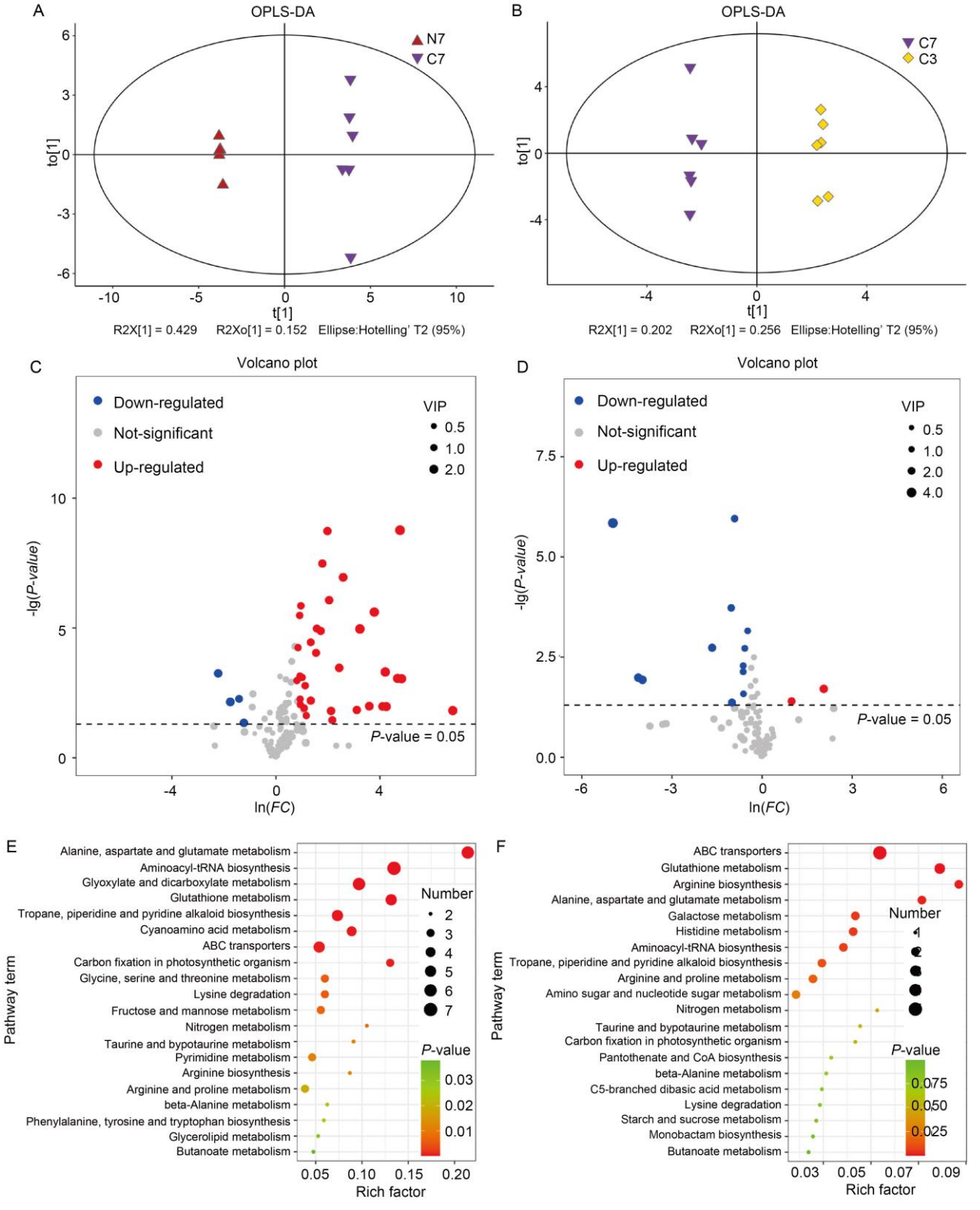

Fig. 2. Analysis of differentially synthesized metabolites (DSMs) based on gas chromatography-mass spectrometer (GC-MS).

A and **B**, Orthogonal Partial least squares-discriminant analysis (OPLS-DA) of NH_4^+-Wuyunjing 7 (N7)/CK-Wuyunjing 7 (C7) (**A**) and C7/CK-Wuyunjing 3 (C3) (**B**).

C and **D**, Volcano plot of DSMs of N7/C7 (**C**) and C7/C3 (**D**). Each point in the volcano plot indicates an identified metabolite, and the red/blue/grey dots indicate up-/down-/non-regulated metabolites. VIP, Variable importance of projection.

E and **F**, Kyoto Encyclopedia of Genes and Genomes analysis of DSMs in N7/C7 (**E**) and of C7/C3 (**F**). *X*-axes represent the pathway item and *Y*-axes represent the rich factor, respectively. The size and color of the dots indicate the number of DSMs and the significance ($P < 0.05$), respectively.

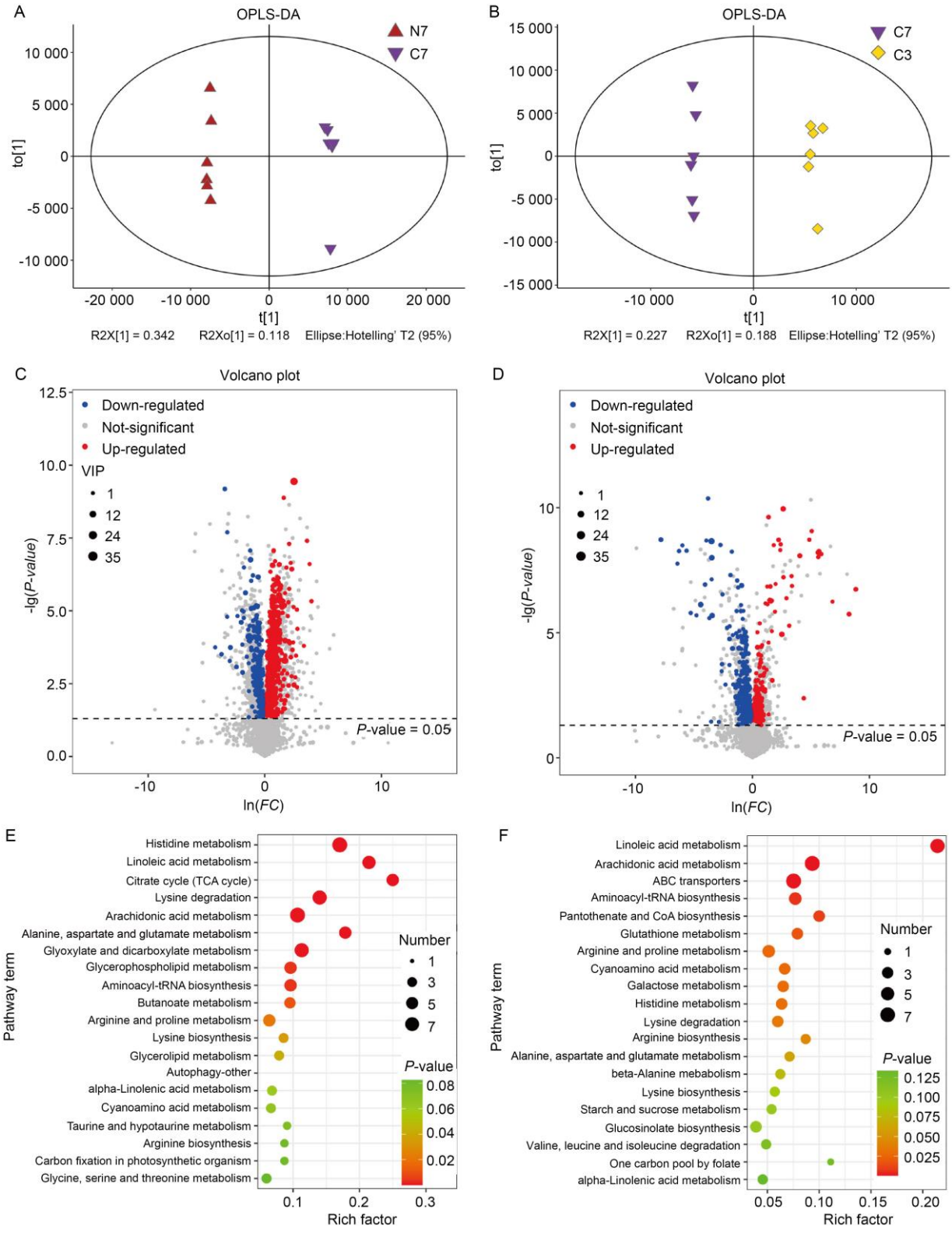

Fig. 3. Analysis of differentially synthesized metabolites (DSMs) based on liquid chromatography-mass spectrometer (LC-MS).

A and **B**, Orthogonal Partial least squares-discriminant analysis (OPLS-DA) of NH_4^+-Wuyunjing 7 (N7)/CK-Wuyunjing 7 (C7) (**A**) and C7/CK-Wuyunjing 3 (C3) (**B**).

C and **D**, Volcano plot of DSMs of N7/C7 (**C**) and C7/C3 (**D**). Each point in the volcano plot indicates an identified metabolite, and the red/blue/grey dots indicate up-/down-/non-regulated metabolites. VIP, Variable importance of projection.

E and **F**, Kyoto Encyclopedia of Genes and Genomes analysis of DSMs in N7/C7 (**E**) and of C7/C3 (**F**). *X*-axes represent the pathway item and *Y*-axes represent the rich factor, respectively. The size and color of the dots indicate the number of DSMs and the significance ($P < 0.05$), respectively.

biosynthesis and secretion, we sequenced nine samples (C7, N7, and C3, with three replicates) using RNA-seq technology, and the RawReads and CleanReads are shown in Table S5. The total mapped reads were more than 90% (Table S5). Totally 800 and 1 308 differentially expressed unigenes (DEGs) were up-regulated and 832 and 2153 DEGs were down-regulated, based on the analysis of N7/C7 and C7/C3 (Table S6). Additionally, 90 (24 is $P < 0.05$) and 91 (17 is $P < 0.05$) GO (Gene Ontology) tested terms of N7/C7 and C7/C3 were divided into three categories, including biological process, cellular component, and molecular function. The largest subcategory of biological process was metabolic process, and cell and catalytic activity

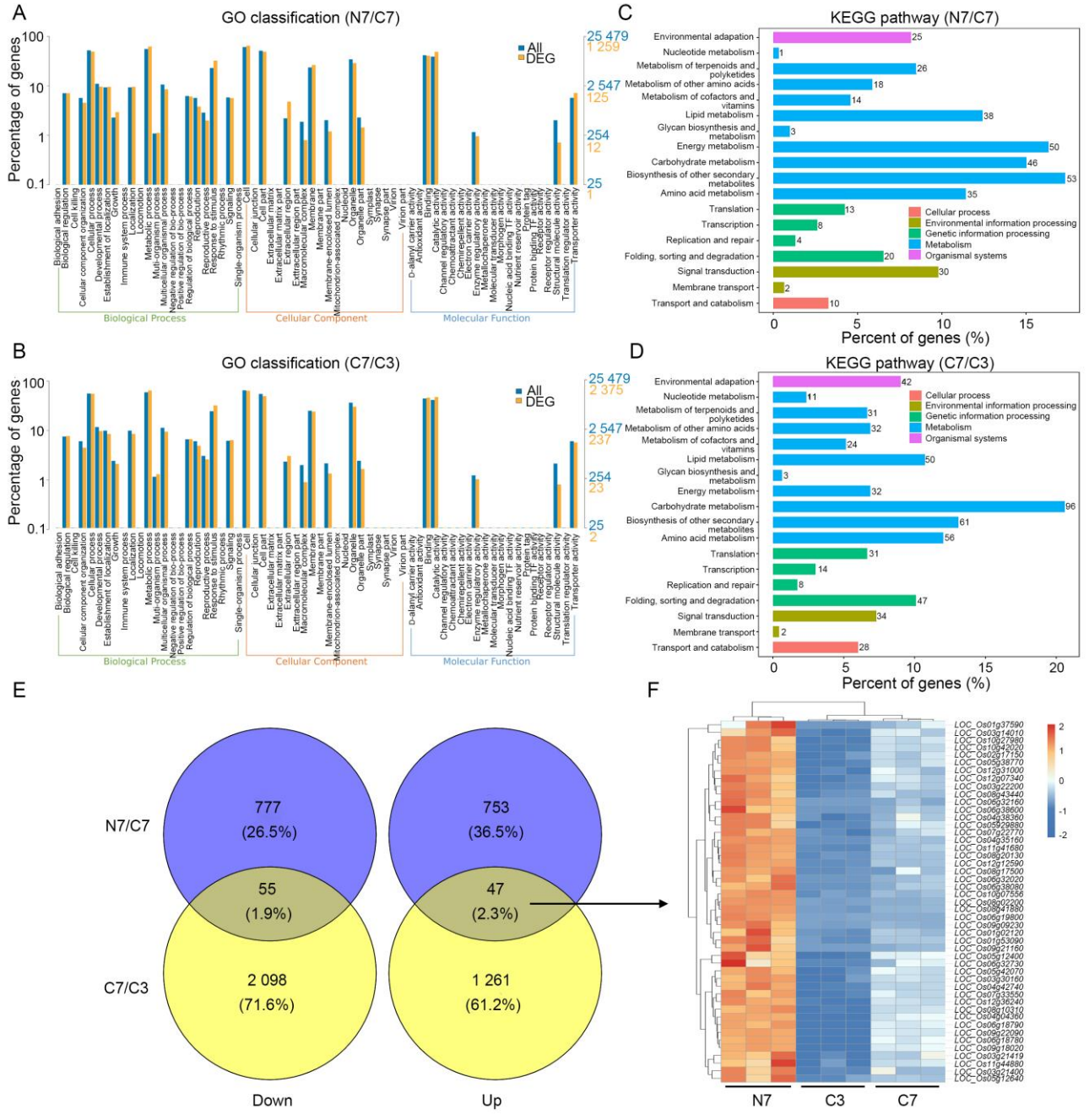

Fig. 4. Analysis of differentially expressed unigenes (DEGs) based on RNA-seq analysis.

A and **B**, Gene Ontology (GO) classification of DEGs in NH_4^+-Wuyunjing 7 (N7)/CK-Wuyunjing 7 (C7) (**A**) and C7/CK-Wuyunjing 3 (C3) (**B**).

C and **D**, Kyoto Encyclopedia of Genes and Genomes (KEGG) enrichment analysis of DEGs in N7/C7 (**C**) and of C7/C3 (**D**).

E, Venn diagram showing co-regulated DEGs in N7/C7 and C7/C3.

F, Hierarchical clustering heatmap of co-upregulated DEGs in N7/C7 and C7/C3.

were the largest subcategories of cellular component and molecular function (Fig. 4-A and -B; Table S7). KEGG enrichment analysis was used to identify the biosynthetic pathways of bioactive components in N7/C7 and C7/C3, 477 and 730 DEGs were annotated into five categories, namely cellular process, environmental information processing, genetic information processing, metabolism, and organismal systems, which further divided into 23 and 19 subcategories (Fig. 4-C and -D; Table S8). Of these subcategories, carbohydrate metabolism (60/135), lipid metabolism (56/64), amino acid metabolism (49/85), biosynthesis of other secondary metabolites (56/68), and signal transduction (43/49) were correlated to more DEGs compared with the other subcategories in N7/C7 and C7/C3, respectively (Table S8).

To further identify the common DEGs in the N7/C7 and C7/C3 groups, we performed Venn analysis and calculated the co-upregulated and -downregulated DEGs (Fig. 4-E). There were 55 co-downregulated and 47 co-upregulated DEGs in N7/C7 and C7/C3. As we sought to identify genes positively associated with enhanced 1,9-D release, we then focused mainly on co-regulated genes. The GO test suggested that these 47 co-upregulated DEGs mainly associated in catalytic activity, metabolic process, and response to stress (Fig. 4-E and Table S9). Furthermore, KEGG enrichment analysis showed that these DEGs were divided into several pathways, including diterpenoid biosynthesis, fatty acid degradation-linolenic acid metabolism, phenylpropanoid biosynthesis and fructose and mannose metabolism (Fig. 4-F and Table S9).

Integrated analysis of metabolome and transcriptome in two experimental groups, N7/C7 and C7/C3

To further examine potential target genes, we performed a Spearman's correlation analysis between DEGs ($P < 0.05$) and DSMs ($P < 0.05$) in N7/C7 and C7/C3 groups (Fig. 5-A and -B). To clarify which DEGs were co-regulated in N7/C7 and C7/C3, we then conducted the Venn analysis and one co-upregulated gene and one co-downregulated gene among 13 co-regulated DEGs

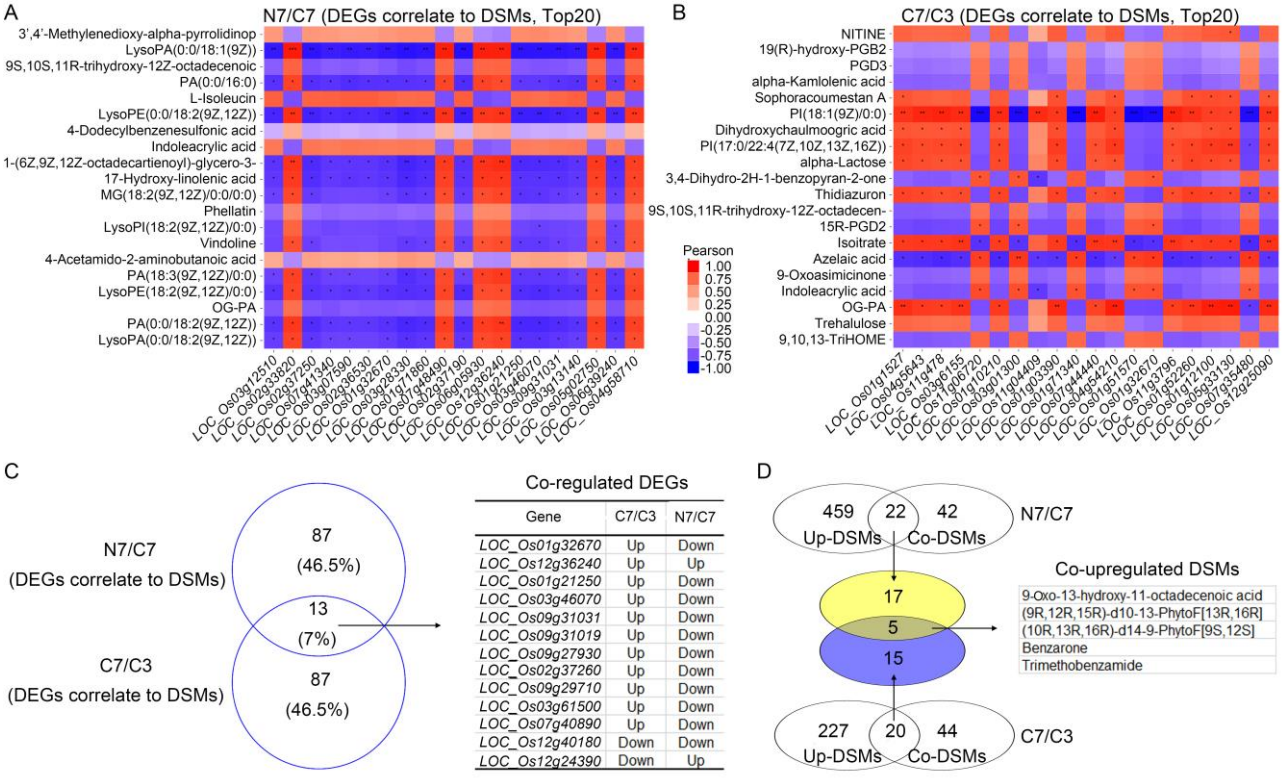

Fig. 5. Identification of co-regulated differentially expressed unigenes (DEGs) and differentially synthesized metabolites (DSMs) via integrated analysis of the metabolome and transcriptome.

A and **B**, Correlation analysis of top 20 DEGs and DSMs in NH_4^+-Wuyunjing 7 (N7)/CK-Wuyunjing 7 (C7) (**A**) and C7/CK-Wuyunjing 3 (C3) (**B**). Red/blue represents a positive/negative correlation. *, ** and *** represent 0.05, 0.01, and 0.001 levels, respectively.

C, Venn analysis of co-regulated DEGs of top 100 correlation between DEGs and DSMs in N7/C7 and C7/C3.

D, Venn analysis of co-upregulated DSMs in N7/C7 and C7/C3.

(Fig. 5-C). The co-upregulated DEG *LOC_Os12g36240* encoded an uncharacterized protein belonging to inhibitor I protein family, while the co-downregulated DEG *LOC_Os12g40180* encoded an unknown protein (Table S10). To further explore which DSMs were responsible for the response to NH_4^+ treatment and variety differences, we then first screened the up-regulated DSMs that were identified as associated DEGs in N7/C7 and C7/C3 groups via the Venn analysis. We identified 22 and 20 up- regulated DSMs with correlated DEGs in N7/C7 and C7/C3 groups, respectively (Fig. 5-D). In a further Venn analysis for these DSMs, we screened five co-upregulated DSMs, namely 9-oxo-12-hydroxy-11-octadecenoic acid, (9R, 12R,15R)-d10-13-PhytoF[13R,16R], (10R,13R,16R)-d14-9-PhytoF[9S,12S], benzarone, and trimethobenzamide (Fig. 5-D). Of these five DSMs, 9-oxo-12-hydroxy-11-octadecenoic acid, (9R,12R,15R)-d10-13-PhytoF [13R,16R], and (10R,13R,16R)-d14-9-PhytoF[9S,12S] were all divided into octadecanoids (Table S2).

Identification of possible metabolites and their associated genes in rice

We then analyzed the boxcharts of three selected DSMs, and found that the relative levels of these three DSMs were the least in CK-WYJ3 and the most in NH_4^+-WYJ7, consistent with the level of 1,9-D, revealing the potential role of octadecanoids during 1,9-D biosynthesis (Figs. 1 and 6-A). To identify the related genes involved in biosynthesis of these three DSMs, we then screened the associated genes from 'DSMs correlation to DEGs' data and found four up-regulated genes, *LOC_Os06g07250*, *LOC_Os07g18750*, *LOC_Os09g29710*, and *LOC_Os11g31090*, in the N7/C7 and C7/C3 groups (Table S10).

To verify the reliability of the RNA-seq data, we further analyzed the transcriptional levels of genes responsible for these three DSMs by qRT-PCR. The transcription patterns of selected genes were similar to the RNA-seq analysis, indicating that the data obtained from RNA-seq were reliable (Fig. 6-B).

Screening of possible genes encoding 1,9-D secretion vectors by RNA-seq data

In addition to the biosynthesis ability, the amount of the secretory carrier also affects the release of 1,9-D. To identify the potential genes involved in regulating 1,9-D release, we first screened the up-regulated transporter-related DEGs in the N7/C7 and C7/C3 groups, and found 40 and 22 DEGs in N7/C7 and C7/C3, respectively (Fig. 7-A and -B). Functional description showed that these DEGs were divided into several transporter families, such as the ATP-binding cassette (ABC) protein family, the multidrug and toxic

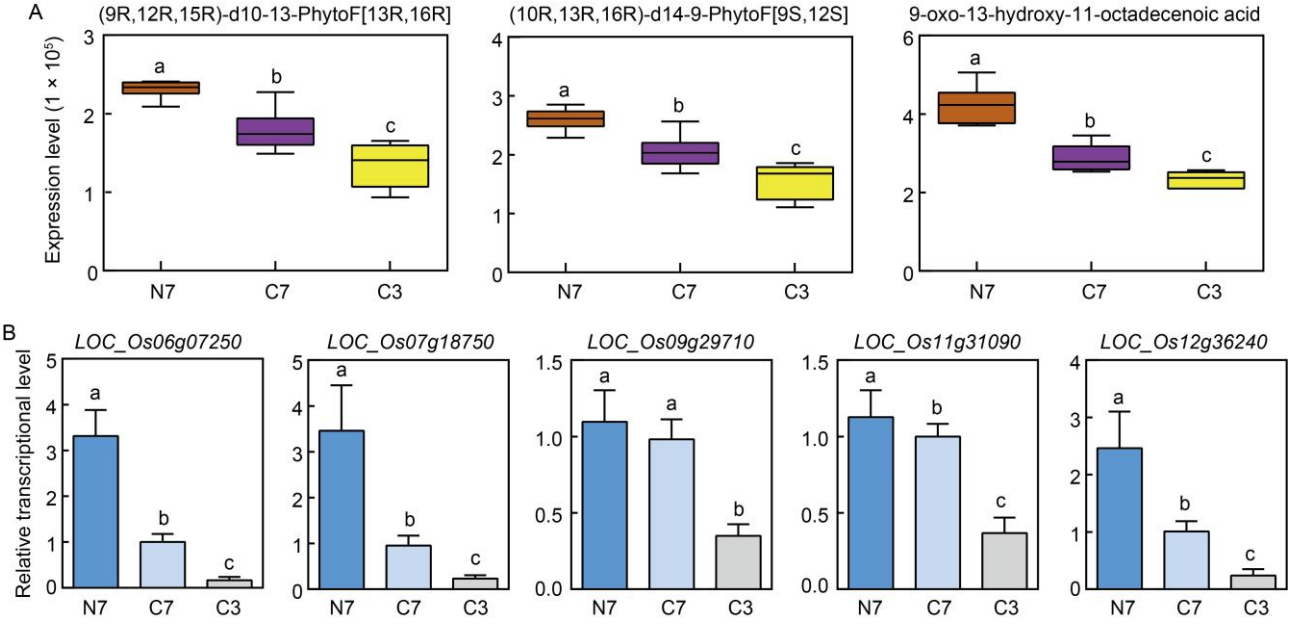

Fig. 6. Identification of possible genes involved in co-upregulated differentially expressed unigenes (DEGs) via qRT-PCR.

A, Boxchart of three co-upregulated metabolites.

B, qRT-PCR analysis of possible genes associated to DEGs.

N7, C7 and C3 represent NH_4^+-Wuyunjing 7, CK-Wuyunjing 7 and CK-Wuyunjing 3, respectively. Values indicate Mean ± SD of three biological replicates. Error bars with different lowercase letters represent statistically significant differences ($P < 0.05$, Duncan's test).

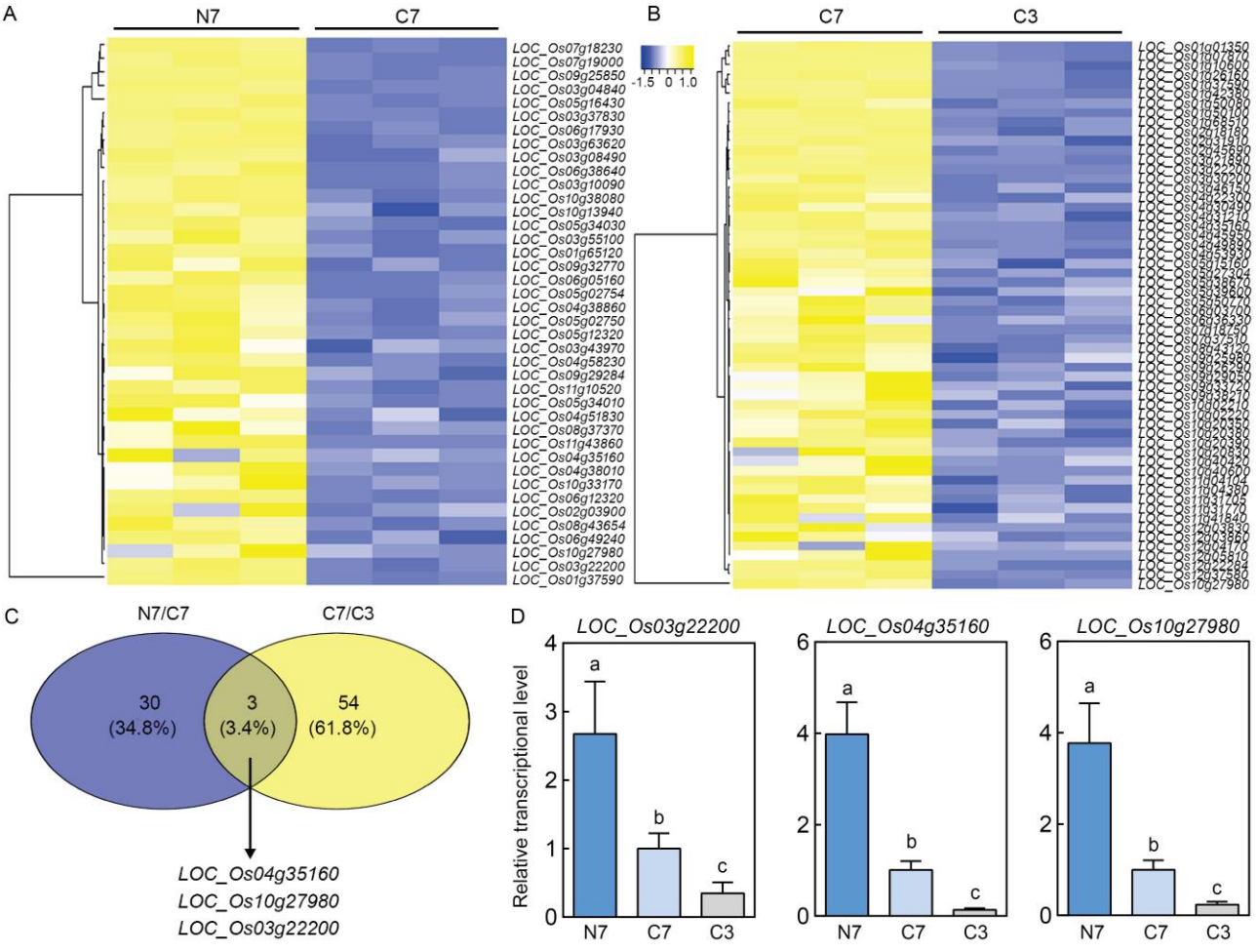

Fig. 7. Identification of possible 1,9-decanediol secretion-related genes.

A and **B**, Hierarchical clustering heatmap of co-upregulated transporter-related differentially expressed unigenes (DEGs) in NH_4^+-Wuyunjing 7 (N7)/CK-Wuyunjing 7 (C7) (**A**) and C7/CK-Wuyunjing 3 (C3) (**B**).

C, Venn analysis of co-upregulated transporter-related genes in N7/C7 and C7/C3.

D, qRT-PCR analysis of co-upregulated genes. Values indicate Mean ± SD of three biological replicates. Error bars with different lowercase letters represent statistically significant differences ($P < 0.05$, Duncan's test).

compound extrusion (MATE) family, and the peptide transporter family (Table S11). Further Venn analysis identified three co-upregulated genes in N7/C7 and C7/C3, including *LOC_Os04g35160*, *LOC_Os10g27980*, and *LOC_Os03g22200*. Subsequent qRT-PCR analysis also identified that transcription levels of these four genes were induced by NH_4^+ treatment in WYJ7 and were inhibited in C3 compared with C7 (Fig. 7-D).

DISCUSSION

BNIs released by roots can effectively suppress bacterial nitrification in a variety of soils, including agricultural soils, leading to the stabilization of the NH_4^+ form of N and allowing plants to use NH_4^+ directly while reducing N loss from soils through NO_3^- leaching and N_2O emission (Subbarao et al, 2006; Coskun et al, 2017b; Zhang M X et al, 2022). The identification and functional analysis of BNIs have been successful in sorghum, pasture grasses, rice, maize, and wheat (Subbarao et al, 2007, 2009; Zakir et al, 2008; O'Sullivan et al, 2016; Sun et al, 2016). BNIs release from roots of these plants decrease both ammonia-oxidizing bacteria and archaea abundance in the rhizosphere, greatly reducing overall soil-bacterial nitrification (Lu et al, 2019; Nardi et al, 2020). However, it has remained unclear how BNIs are synthesized *in vivo* and by what mechanisms they are secreted into the rhizosphere (Zhang M X et al, 2022). Due to the pronounced differences in 1,9-D secretion in different rice varieties (WYJ3 and WYJ7) and in response to NH_4^+ treatment (Fig. 1), we have here used this as a basis for a multi-omics screen, with the

goal of pinpointing possible biosynthetic pathways and transporters that may be engaged in 1,9-D secretion.

Are 'fatty acids' pathways responsible for 1,9-D biosynthesis in rice?

Our previous study showed that 1,9-D is a C10 fatty alcohol (Sun et al, 2016). Fatty alcohols are composed of a non-polar, lipophilic carbon chain (C8–C18) and a polar, hydrophilic hydroxyl group. In engineered microbes, the biosynthesis of fatty alcohols begins with the formation of fatty acyl-acyl carrier proteins (FA-ACPs) (Zheng et al, 2012). FA-ACPs are then converted to free fatty acids and fatty acyl coenzyme A (FA-CoA), in a series of reactions catalyzed by thioesterase and acyl-CoA synthase (Lu et al, 2008). FA-CoA is then reduced to fatty aldehydes or fatty alcohols in an NADPH-dependent manner, catalyzed by fatty acyl-CoA reductase. In turn, fatty aldehydes can also be converted to fatty alcohols by alcohol dehydrogenases or aldehyde reductases (Reiser and Somerville 1997; Vioque and Kolattukudy 1997). Thus, thioesterase, acyl-CoA synthase, and fatty acyl-CoA reductase are key enzymes in fatty alcohol biosynthesis (Steen et al, 2010). Interestingly, these enzymes can differ significantly in substrate specificity (Liu et al, 2011).

To screen for metabolites and genes positively associated with 1,9-D biosynthesis, we performed a Spearman correlation analysis between DEGs (P < 0.05) and DSMs (P < 0.05) in the N7/C7 and C7/C3 groups and chose the Top 100 for further investigation (Fig. 5-A and -B). KEGG enrichment data showed that these DEGs and DEMs were enriched in 58 and 49 metabolic pathways in N7/C7 and C7/C3, respectively, and that 42 metabolic pathways were co-enriched in these two groups (Table S6). Venn analysis identified the co-upregulated DEGs and found 13 co-regulated DEGs, of which only one DEG was co-upregulated and one DEG was co-down-regulated in N7/C7 and C7/C3 (Fig. 5-C). Subsequent 'Gene Function Annotation' suggested that these two DEGs may not be potential genes related to 1,9-D biosynthesis (Table S6). A further screen of the co-upregulated DSMs in N7/C7 and C7/C3 revealed five co-upregulated DSMs (Fig. 5-D). Of these five DSMs, 9-oxo-12-hydroxy-11-octadecenoic acid, (9R, 12R,15R)-d10-13-PhytoF[13R,16R], and (10R,13R,16R)-d14-9-PhytoF[9S,12S] fall into the category of linoleic acid metabolism (osa00591), and, more generally, involvement in the metabolism of octadecanoids, i.e. C18 fatty acids, was indicated (Fig. 5-D and Table S6). Octadecanoids have been described as signaling compounds induced under stress such as in response to wounding and in the context of plant defense (Fliegmann et al, 2003). However, whether the octadecanoids involved in such responses are also the synthetic precursors of 1,9-D remains unclear. Our data showed that three metabolites associated with octadecanoid metabolism and their associated genes are distinctly up-regulated in the N7/C7 and C7/C3 groups, respectively (Fig. 6).

We further analyzed the enriched metabolic pathways (KEGG enrichment) via Top 100 correlation analysis (P < 0.05). The DSMs involved in cutin, suberin, and wax biosynthesis (osa00073), α-linolenic acid metabolism (osa00592), and biosynthesis of unsaturated fatty acids (osa01040), all of which are implicated in fatty acid metabolism, were up-regulated in C7/C3, but not in N7/C7. This indicates that the differences in 1,9-D content between the two varieties (WYJ7 *vs* WYJ3) and the differences in 1,9-D content following NH_4^+ application (NH_4^+ *vs* CK in WYJ7) are accomplished via different metabolic pathways (Fig. 8 and Table S6). In the context of the above DSMs, it is instructive to point out that linolenic acid and linoleate were also isolated from, and identified in, *Brachiaria humidicola* shoots as BNIs. These compounds are capable of blocking the activities of AMO and hydroxylamino oxidoreductase in *Nitrosomonas* (Subbarao et al, 2008). Additionally, the fatty acids palmitic acid and oleic acid, which may also be involved in 1,9-D biosynthesis, have been reported to block AMO activity in *Nitrosomonas* at higher concentrations (Subbarao et al, 2008) (Fig. 8). These findings suggest important roles of these plant-metabolic pathways in inhibiting bacterial nitrification.

Much work remains to be done to establish definitively which metabolic pathway components are involved in the biosynthesis of 1,9-D, both at the biochemical and genetic levels. To achieve this, the following steps may be effective: (i) exogenous application of candidate metabolites to rice roots coupled to the determination of the amount of 1,9-D exudation in response to each; (ii) application of Crispr/Cas9 and/or gene overexpression techniques to knock out or upregulate genes in relevant metabolic pathways coupled to the determination of the amount of 1,9-D exudation in transgenic material.

Which transporters are responsible for the transport of 1,9-D in rice roots?

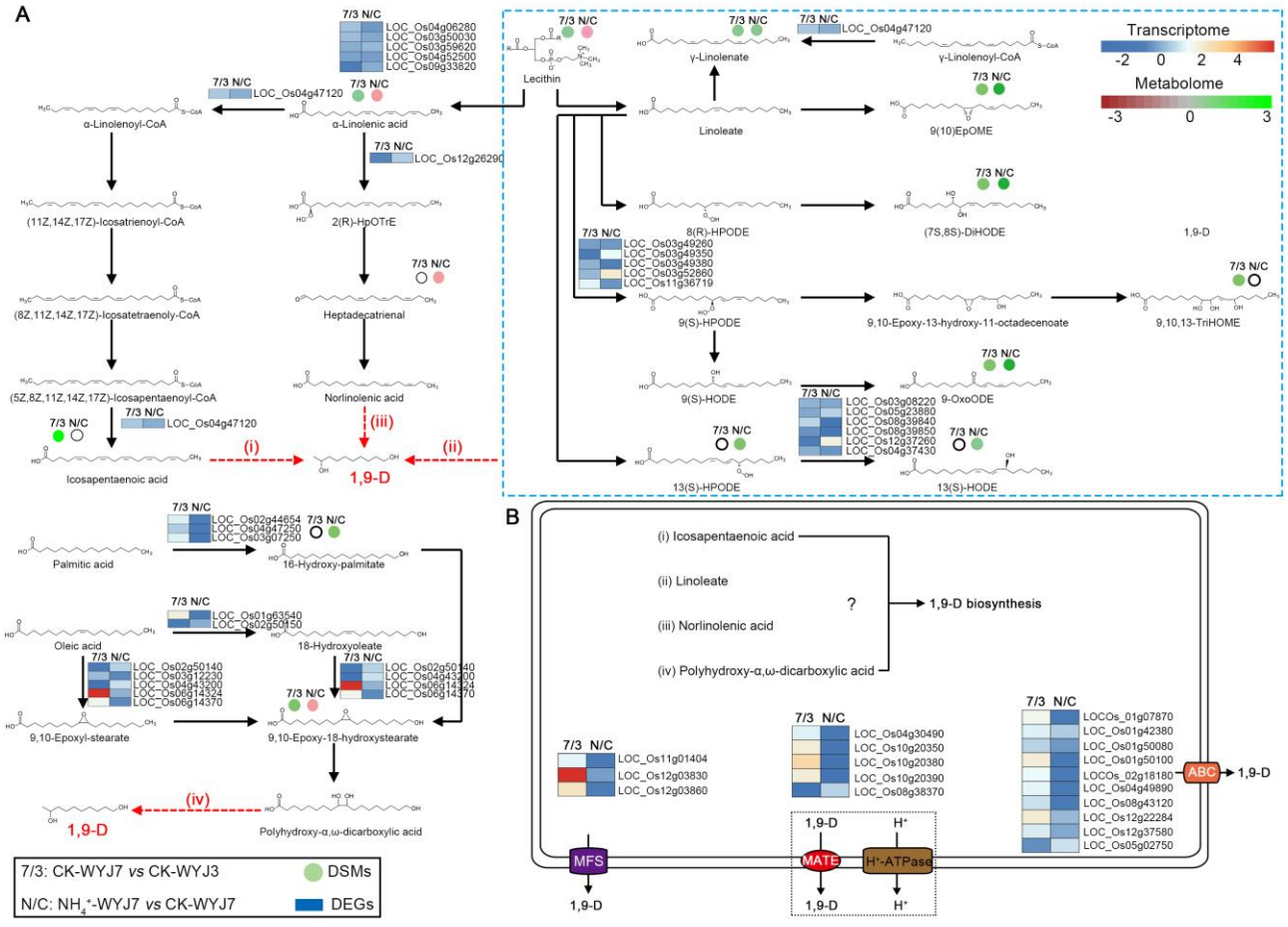

Fig. 8. Potential biosynthesis pathways and transporters responsible for 1,9-decanediol (1,9-D) synthesis and release in rice.
A, Potential metabolic pathways involved in 1,9-D biosynthesis.
B, Potential transporters responsible for 1,9-D release.
MATE,Major facilitator superfamily; MFS, ATP-binding cassette protein family; ABC, Multidrug and toxic compound extrusion family.

BNIs can be divided into hydrophilic and hydrophobic BNIs, according to the compounds' solubility in water (Zhang M X et al, 2022). For hydrophobic BNIs, e.g. sorgoleone, the release from roots can occur through exocytosis and/or vesicle trafficking (Czarnota et al, 2003). By contrast, the release of hydrophilic BNIs may be mediated by voltage-gated anion channels and/or transporters (Zhang M X et al, 2022). To find the carriers or channels responsible for the release of 1,9-D into the rhizosphere, we performed RNA-seq analysis in CK-WYJ3 (no 1,9-D release), CK-WYJ7 (high 1,9-D release), and NH_4^+-WYJ7 (higher 1,9-D release), and then identified up-regulated DEGs categorized into the transporter ability GO item, in the two groups, C7/C3 and N7/C7 (Fig. 7 and Table S11).

We screened 34 and 58 up-regulated DEGs in the C7/C3 and N7/C7 groups, respectively (Fig. 7-A and -B). Venn analysis then suggested that the two groups shared the same three DEGs, namely *LOC_Os03g22200*, *LOC_Os04g35160*, and *LOC_Os10g27980* (Fig. 7-C). *LOC_Os04g35160* encodes a CorA-like magnesium transporter protein that may have the same magnesium transport capacity as its homologous protein LOC_Os01g64890 (OsMGT1) (Chen et al, 2012). LOC_Os03g22200 (OsSWEET16), a nodulin MtN3 family protein, functions as a sugar transporter and is involved in responses to plant pathogen infection (Streubel et al, 2013). The protein encoded by *LOC_Os10g27980* belongs to a family of transmembrane amino acid transport proteins, of which several auxin influx transporters, including AUX1-5, are the most extensively studied (Yu et al, 2015; Zhao et al, 2015; Wang et al, 2019; Ye et al, 2021). However, based on available results, we were unable to confirm whether the proteins encoded by these three genes are involved in the release of 1,9-D.

In addition, four main classes of transporter proteins currently thought to be involved in the release of

metabolite release from roots to the rhizosphere are the ABC protein family, the MATE family, the major facilitator superfamily (MFS), and the aluminum-activate malate transporter (ALMT) family (Weston et al, 2012; Zhang M X et al, 2022). ABC transporters show wide distribution among higher plants and are involved in the secretion of secondary metabolites from roots (Martinoia et al, 2002; Buer et al, 2007; Badri et al, 2008; Zhang M X et al, 2022). BNI release from sorghum roots is suppressed by the ABC transporter inhibitor vanadate (Rea 2007; Coskun et al, 2017a; Zhang M X et al, 2022), supporting a potential role for ABC transporters in BNI release. MATE proteins are responsible for citrates, benzoxazoles, artemisinins, inulin, phenols, alkaloids, and flavonoids, the transport of which depends on counterion gradients, typically the trans-plasma-membrane gradient of H^+. MHPP and sakuranetin released from sorghum roots are a phenolic and a flavonoid, respectively, potential transport substrates for MATE, while the activity of plasma membrane H^+-ATPases clearly affects the release of BNIs from sorghum roots, underscoring the importance of proton coupling in BNI transport (Shen et al, 2005; Furukawa et al, 2007; Zhao and Dixon 2009; Zeng et al, 2016; Doshi et al, 2017). Taken together, the available data suggest that MATE transporters are involved in the release of BNIs (Sivaguru et al, 2013; Doshi et al, 2017). Members of the MFS protein family can function as antiporters, co-transporters, and uniporters. In rice, one MFS protein, TOM1, mediates deoxymugineic and avenic acid release from roots, suggesting a possible role of MFS proteins during BNI release as well (Nozoye et al, 2011; Weston et al, 2012). The ALMT protein is implicated in aluminum resistance by mediating malate ion release from roots to the rhizosphere, but whether it can also serve as a transporter of 1,9-D needs to as yet be ascertained (Ryan et al, 2011; Weston et al, 2012).

Interestingly, among the enriched and up-regulated genes in C7/C3, there were nine genes encoding ABC proteins, including *LOC_Os01g07870* (*ABCC3*), *LOC_Os01g42380* (*ABCG35*), *LOC_Os01g50080* (*ABCB21*), *LOC_Os01g50100* (*ABCB10*), *LOC_Os04g49890* (*ABCC9*), *LOC_Os02g18180* (*ABCE1*), *LOC_Os08g43120* (*ABCG48*), *LOC_Os12g22284* (*ABCG3*), and *LOC_Os12g37580* (*ABCC10*), four genes encoding MATE proteins, such as *LOC_Os04g30490*, *LOC_Os10g20350*, *LOC_Os10g20380* and *LOC_Os1020390*, and three MFS protein-related genes, *LOC_Os11g04104*, *LOC_Os12g03830*, and *LOC_Os12g03860* (Fig. 7-A to -C and Table S11). By contrast, only one ABC transporter, STAR2 (LOC_Os05g02750), and one MATE transporter, LOC_Os08g39370, were identified and seen as up-regulated in the N7/C7 group, and the results were corroborated by qRT-PCR analysis (Fig. S4). Whether the transporters responsible for 1,9-D release from different rice varieties are different from those induced by NH_4^+ is an interesting question and a worthy subject for further research.

To further pinpoint which transporters play key roles in 1,9-D release, we suggest the following: (i) ectopic expression of the transporters in frog oocytes and determination of 1,9-D secretion; (ii) application of CRISPR/Cas9 and gene over-expression motifs to construct knockout and overexpressed transgenic rice lines and measurement of 1,9-D release in these lines to clarify the roles of various gene candidates in regulating 1,9-D secretion.

In summary, we here performed a multi-omic analysis to identify candidate genes involved in 1,9-D biosynthesis and transport. We found that the regulation of 1,9-D release in different genotypes (WYJ7 and WYJ3) and in response to NH_4^+ treatments may not employ the same biosynthetic pathways and transporters. In future work, we hope to identify linkage regions associated with 1,9-D release by genome-wide association analysis of rice varieties with different 1,9-D-secretion abilities or by detection of QTLs for 1,9-D release from WYJ7/WYJ3 populations. Joint analysis of candidate genes obtained by multi-omic analysis and linkage regions identified by GWAS and QTLs, as well genetic transformation of callus tissue, should assist in definitively efficient pinpointing the genes implicated in 1,9-D biosynthesis and those governing its release from roots.

METHODS

Plant materials and growth conditions

Two rice varieties, WYJ7 (high 1,9-D release) and WYJ3 (no 1,9-D release), were used. Seeds were surface-sterilized with 3% H_2O_2 for 1 h, rinsed with distilled water three times, and then germinated on 0.5 mmol/L $CaCl_2$ at 30 ℃ for 2 d. Subsequently, germinated seeds were transferred into 1/2 modified Kimura solution for a 4-day pretreatment; the solution composition was as follows: 0.5 mmol/L NH_4NO_3, 0.18 mmol/L KH_2PO_4, 0.54 mmol/L $MgSO_4$ $7H_2O$, 0.18 mmol/L KCl, 0.36 mmol/L $CaCl_2$, 0.2 μmol/L $CuSO_4$ $5H_2O$, 0.5 μmol/L $MnCl_2$ $4H_2O$, 0.4 μmol/L $ZnSO_4$ $7H_2O$, 3 μmol/L H_3BO_3, 1 μmol/L $(NH_4)_6Mo_7O_{24}$ $4H_2O$, and 20 μmol/L Na_2EDTA-Fe. The solution pH was 5.8. Seedlings were cultivated in a growth chamber, with a 16 h/8 h and 30 ℃/

28 ℃ light/dark cycle, 400 μmol/(m^2 s) light intensity, and a relative humidity of 65%. The root exudates were collected from 6-week-old seedling roots (Zhang et al, 2019; Lu et al, 2022).

Root exudate collection and 1,9-D determination

Thirty 6-week-old seedlings (n = 4) from each replicate were rinsed three times consecutively with deionized water prior to use. The washed seedlings were then transferred to a tall, light-proof glass beaker and the roots were gently immersed in 1 L of 1.0 mmol/L NH_4Cl or 1.0 mmol/L $CaCl_2$ and assayed for 1,9-D release. The detailed collection method and test procedure were described in our previous study (Zhang et al, 2019).

Metabolite identification using GC-MS and data analysis

Accurately weighed samples (60 mg) and two small steel balls were added to a 1.5-mL tube. Methanol and water mixture (1:1, containing L-2-chlorophenylalanine of 4 μg/mL) of 600 μL were added and then placed at -40 ℃ for 2 min. Subsequently, the samples were ground at 60 Hz for 2 min and then extracted by ultrasonic for 30 min in ice-water. Chloroform1 (50 μL) was added to the samples and vortexed for another 2 min. The samples were extracted by ultrasonic for 30 min in ice-water bath, then placed at -40 ℃ for 30 min and centrifuged at 4 ℃ (13 000 r/min) for 10 min. Supernatant (150 μL) was collected in a glass vial and dried in a freeze-concentration centrifugal dryer, then 80 μL of 15 mg/mL methoxylamine hydrochloride in pyridine was added and the mixture was incubated at 37 ℃ for 60 min. Then, 50 μL of Bis(trimethylsilyl)-trifluoroacetamide (with 1% Trimethylchlorosilane and 20 μL n-hexane were added into the mixture, and then derivatized at 70 ℃ for 60 min. The samples were further placed at ambient temperature for 30 min prior to GC-MS analysis.

The above samples were further analyzed on an Agilent 7890B gas chromatography system coupled to an Agilent 5977B MSD system (Agilent Technologies Inc., CA, USA). An AHP-5MS fused-silica capillary column (30 m × 0.25 mm × 0.25 μm, Agilent J & W Scientific, Folsom, CA, USA) was utilized to separate the derivatives. The original data were imported into the MS-DIAL software and further characterized based on the LUG database. Subsequently, principle component analysis, OPLS-DA and partial least squares-discriminant analysis (PLS-DA) were utilized to observe and distinguish the overall distribution among the samples and the stability of analysis. To prevent overfitting, 7-fold cross-validation and 200 RPT were used to evaluate the quality of the model. Variable importance of projection (VIP) values obtained from the OPLS-DA model and two-tailed Student's t-test was further used to rank the overall contribution of each variable and to verify whether the differences in metabolites between groups were significant. DEMs were selected with VIP > 1.0 and P < 0.05.

Metabolite identification using LC-MS and data analysis

Root samples (60 mg) and two small steel balls were added to the tube. Methanol and water mixture (7:3, containing L-2-chlorophenylalanine of 4 μg/mL) of 600 μL were added to each sample and placed at -40 ℃ for 2 min. Then, the samples were ground at 60 Hz for 2 min, and further extracted by ultrasonic for 30 min in an ice-water bath, and placed overnight at -40 ℃. Samples were centrifuged at 4 ℃ (13 000 r/min) for 10 min, and the 150-μL supernatants were collected from each tube using crystal syringes. The samples were filtered through 0.22-μm microfilters and transferred to LC vials prior to determination.

The samples were analyzed using an ACQUITY UPLC I-Class system (Waters corporation, Milford, USA) coupled to a VION IMS QTOF mass spectrometer (Waters Corporation, Milford, USA). The original LC-MS data were processed using the Progenesis QI V2.3 software (Nonlinear, Dynamics, Newcastle, UK) and qualitatively analyzed by using The Human Metabolome Database (HMDB), Lipidmaps (V2.3), Metlin, EMDB, PMDB, and self-built databases. Subsequently, data quality control used the same metrics as were used in GS-MS. The valid DEMs were selected with VIP > 1.0 and P < 0.05.

RNA extraction and RNA-sequencing

Total RNA samples were extracted using a mirVana™ miRNA Isolation Kit (QIAGEN, Darmstadt, Germany) following the manufacture's protocol. The quality of RNA was evaluated using an Agilent 2100 Bioanalyzer (Agilent Technologies, Santa Clara, CA, USA). The detailed methods of synthesizing and purifying the first- strand and double-strand cDNA and the sample library construction were as described in our previous studies (Sun et al, 2017, 2020). Subsequently, the library products were sequenced by Illumina Nova6000.

DEGs were analyzed by using the NOISeq method. The valid DEGs were chosen with a threshold of P < 0.05 and an FC value > 2. The Short Time-series Expression Miner (STEM) program (version 1.3.11) was used to construct a hierarchical cluster, which was used to exhibit the expression patterns of genes in different samples. GO enrichment and KEGG pathway enrichment analysis of DEGs were performed using R, as also described in detail in our previous studies (Sun et al, 2017, 2020).

Integrated analysis of DSMs and DEGs

The Pearson's correlation test was performed to screen the correlations between the DSMs and DEGs (P < 0.05) (https://cloud.oebiotech.cn/task/). Subsequently, DEGs and DSMs were further mapped to the KEGG database and their common pathway information was thus obtained.

qRT-PCR

The total RNA was extracted by using the FastPure Universal Plant Total RNA Isolation Kit (RC411, Vazyme Biotech Co., Ltd, Nanjing, China). Total RNA (500 ng) was used for reverse transcription by using a HiScript 1st-Strand cDNA Synthesis

Kit (R111; Vazyme Biotech Co., Ltd, Nanjing, China) and then cDNA was diluted (20 times) prior to qRT-PCR analysis. The qRT-PCR program was as described (Di et al, 2018). The primers are listed in Table S1.

Statistical analysis

Data were analyzed using the Prism 6 software (GraphPad Software). Student's *t*-test was performed to compare between the two groups. *P*-values denote significant differences (*, $P < 0.05$; **, $P < 0.01$; and ***, $P < 0.001$). One-way analysis of variance tests were used to compare among multiple groups, and $P < 0.05$ was used as the significance cut-off.

ACKNOWLEDGEMENTS

This study was supported by the National Natural Science Foundation of China (Grant Nos. 32030099 and 32072670), the Strategic Priority Research Program of the Chinese Academy of Sciences (Grant No. XDA28020301), the Youth Innovation Promotion Association of the Chinese Academy of Sciences (Grant No. 2023326), and Enterprise Cooperation Projects of China (Grant No. Am20210407RD). We thank Shanghai OE Biotech Co., Ltd and Shanghai Luming Biological Technology Co., Ltd for transcriptome and metabolome analyses.

SUPPLEMENTAL DATA

The following materials are available in the online version of this article at http://www.sciencedirect.com/journal/rice-science; http://www.ricescience.org.

Fig. S1. Response sorting tests (200) of orthogonal partial least squares-discriminant analysis (OPLS-DA) model of gas chromatography-mass spectrometer.

Fig. S2. Response sorting tests (200) of orthogonal partial least squares-discriminant analysis (OPLS-DA) model of liquid chromatography-mass spectrometer.

Fig. S3. KEGG analysis of up-regulated and down-regulated differentially synthesized metabolites (DSMs, top20) in N-WYJ7 vs C-WYJ7 and C-WYJ7 vs C-WYJ3.

Fig. S4. Relative transcription of genes encoding 1,9-decanediol transporters in C-WYJ3, C-WYJ7 and N-WYJ7.

Table S1. Differentially synthesized metabolites identified by gas chromatography-mass spectrometer.

Table S2. KEGG analysis of N-WYJ7 vs C-WYJ7 and C-WYJ7 vs C-WYJ3 using gas chromatography-mass spectrometer.

Table S3. Differentially synthesized metabolites identified by liquid chromatography-mass spectrometer.

Table S4. KEGG analysis of N-WYJ7 vs C-WYJ7 and C-WYJ7 vs C-WYJ3 using liquid chromatography-mass spectrometer.

Table S5. Statistics of RNA-seq data.

Table S6. Total differentially expressed unigenes identified in N-WYJ7 vs C-WYJ7 and C-WYJ7 vs C-WYJ3.

Table S7. GO enrichment analysis in N-WYJ7 vs C-WYJ7 and C-WYJ7 vs C-WYJ3.

Table S8. KEGG enrichment analysis in N-WYJ7 vs C-WYJ7 and C-WYJ7 vs C-WYJ3.

Table S9. Co-upregulated genes in N-WYJ7 vs C-WYJ7 and C-WYJ7 vs C-WYJ3.

Table S10. Differentially synthesized metabolites correlated to differentially expressed unigenes in N-WYJ7 vs C-WYJ7 and C-WYJ7 vs C-WYJ3.

Table S11. Up-regulated genes involved in transporter activity in N-WYJ7 vs C-WYJ7 and C-WYJ7 vs C-WYJ3.

Table S12. Primers used in this study.

REFERENCES

Badri D V, Loyola-Vargas V M, Broeckling C D, De-la-Peña C, Jasinski M, Santelia D, Martinoia E, Sumner L W, Banta L M, Stermitz F, Vivanco J M. 2008. Altered profile of secondary metabolites in the root exudates of *Arabidopsis* ATP-binding cassette transporter mutants. *Plant Physiol*, **146**(2): 762–771.

Buer C S, Muday G K, Djordjevic M A. 2007. Flavonoids are differentially taken up and transported long distances in Arabidopsis. *Plant Physiol*, **145**(2): 478–490.

Chen Z C, Yamaji N, Motoyama R, Nagamura Y, Ma J F. 2012. Up-regulation of a magnesium transporter gene *OsMGT1* is required for conferring aluminum tolerance in rice. *Plant Physiol*, **159**(4): 1624–1633.

Cheng H, Kong W P, Tang T X, Ren K L, Zhang K L, Wei H X, Lin T. 2022. Identification of key gene networks controlling soluble sugar and organic acid metabolism during oriental melon fruit development by integrated analysis of metabolic and transcriptomic analyses. *Front Plant Sci*, **13**: 830517.

Coskun D, Britto D T, Shi W M, Kronzucker H J. 2017a. How plant root exudates shape the nitrogen cycle. *Trends Plant Sci*, **22**(8): 661–673.

Coskun D, Britto D T, Shi W M, Kronzucker H J. 2017b. Nitrogen transformations in modern agriculture and the role of biological nitrification inhibition. *Nat Plants*, **3**: 17074.

Czarnota M A, Paul R N, Weston L A, Duke S O. 2003. Anatomy of sorgoleone-secreting root hairs of *Sorghum* species. *Int J Plant Sci*, **164**(6): 861–866.

Di D W, Sun L, Zhang X N, Li G J, Kronzucker H J, Shi W M. 2018. Involvement of auxin in the regulation of ammonium tolerance in rice (*Oryza sativa* L.). *Plant Soil*, **432**(1): 373–387.

Doshi R, McGrath A P, Piñeros M, Szewczyk P, Garza D M, Kochian L V, Chang G. 2017. Functional characterization and discovery of modulators of SbMATE, the agronomically important aluminium tolerance transporter from *Sorghum bicolor*. *Sci Rep*, **7**: 17996.

Elrys A S, Desoky E S M, Abo El-Maati M F, Elnahal A S, Abdo A I, Raza S, Zhou J B. 2019. Can secondary metabolites extracted from *Moringa* seeds suppress ammonia oxidizers to increase nitrogen use efficiency and reduce nitrate contamination in potato tubers? *Ecotoxicol Environ Saf*, **185**: 109689.

Elrys A S, Uwiragiye Y, Zhang Y H, Abdel-Fattah M K, Chen Z X, Zhang H M, Meng L, Wang J, Zhu T B, Cheng Y, Zhang J B, Cai Z C, Chang S X, Müller C. 2023. Expanding agroforestry can

increase nitrate retention and mitigate the global impact of a leaky nitrogen cycle in croplands. *Nat Food*, **4**(1): 109–121.

Fliegmann J, Schüler G, Boland W, Ebel J, Mithöfer A. 2003. The role of octadecanoids and functional mimics in soybean defense responses. *Biol Chem*, **384**(3): 437–446.

Fu M Y, Yang X, Zheng J R, Wang L, Yang X Y, Tu Y, Ye J B, Zhang W W, Liao Y L, Cheng S Y, Xu F. 2021. Unraveling the regulatory mechanism of color diversity in *Camellia japonica* petals by integrative transcriptome and metabolome analysis. *Front Plant Sci*, **12**: 685136.

Furukawa J, Yamaji N, Wang H, Mitani N, Murata Y, Sato K, Katsuhara M, Takeda K, Ma J F. 2007. An aluminum-activated citrate transporter in barley. *Plant Cell Physiol*, **48**(8): 1081–1091.

Kaur-Bhambra J, Wardak D L R, Prosser J I, Gubry-Rangin C. 2022. Revisiting plant biological nitrification inhibition efficiency using multiple archaeal and bacterial ammonia-oxidising cultures. *Biol Fertil Soils*, **58**(3): 241–249.

Kronzucker H J, Siddiqi M Y, Glass A D M. 1997. Conifer root discrimination against soil nitrate and the ecology of forest succession. *Nature*, **385**: 59–61.

Kronzucker H J, Siddiqi M Y, Glass A D, Kirk G J. 1999. Nitrate-ammonium synergism in rice: A subcellular flux analysis. *Plant Physiol*, **119**(3): 1041–1046.

Li T L, Wang Z G, Wang C X, Huang J Y, Feng Y F, Shen W S, Zhou M, Yang L Z. 2022. Ammonia volatilization mitigation in crop farming: A review of fertilizer amendment technologies and mechanisms. *Chemosphere*, **303**: 134944.

Liu X Y, Sheng J, Curtiss R 3rd. 2011. Fatty acid production in genetically modified cyanobacteria. *Proc Natl Acad Sci USA*, **108**(17): 6899–6904.

Lu X F, Vora H, Khosla C. 2008. Overproduction of free fatty acids in *E. coli*: Implications for biodiesel production. *Metab Eng*, **10**(6): 333–339.

Lu Y F, Zhang X N, Jiang J F, Kronzucker H J, Shen W S, Shi W M. 2019. Effects of the biological nitrification inhibitor 1, 9-decanediol on nitrification and ammonia oxidizers in three agricultural soils. *Soil Biol Biochem*, **129**: 48–59.

Lu Y F, Zhang X N, Ma M K, Zu W J, Kronzucker H J, Shi W M. 2022. Syringic acid from rice as a biological nitrification and urease inhibitor and its synergism with 1,9-decanediol. *Biol Fertil Soils*, **58**(3): 277–289.

Ma M K, Lu Y F, Di D W, Kronzucker H J, Dong G Q, Shi W M. 2023. The nitrification inhibitor 1, 9-decanediol from rice roots promotes root growth in *Arabidopsis* through involvement of ABA and PIN2-mediated auxin signaling. *J Plant Physiol*, **280**: 153891.

Martinoia E, Klein M, Geisler M, Bovet L, Forestier C, Kolukisaoglu Ü, Müller-Röber B, Schulz B. 2002. Multifunctionality of plant ABC transporters: More than just detoxifiers. *Planta*, **214**(3): 345–355.

Min J, Shi W M. 2018. Nitrogen discharge pathways in vegetable production as non-point sources of pollution and measures to control it. *Sci Total Environ*, **613/614**: 123–130.

Min J, Sun H J, Wang Y, Pan Y F, Kronzucker H J, Zhao D Q, Shi W M. 2021. Mechanical side-deep fertilization mitigates ammonia volatilization and nitrogen runoff and increases profitability in rice production independent of fertilizer type and split ratio. *J Clean Prod*, **316**: 128370.

Nardi P, Laanbroek H J, Nicol G W, Renella G, Cardinale M, Pietramellara G, Weckwerth W, Trinchera A, Ghatak A, Nannipieri P. 2020. Biological nitrification inhibition in the rhizosphere: Determining interactions and impact on microbially mediated processes and potential applications. *FEMS Microbiol Rev*, **44**(6): 874–908.

Nozoye T, Nagasaka S, Kobayashi T, Takahashi M, Sato Y, Sato Y, Uozumi N, Nakanishi H, Nishizawa N K. 2011. Phytosiderophore efflux transporters are crucial for iron acquisition in graminaceous plants. *J Biol Chem*, **286**(7): 5446–5454.

O'Sullivan C A, Fillery I R P, Roper M M, Richards R A. 2016. Identification of several wheat landraces with biological nitrification inhibition capacity. *Plant Soil*, **404**(1): 61–74.

Otaka J, Subbarao G V, Ono H, Yoshihashi T. 2022. Biological nitrification inhibition in maize: Isolation and identification of hydrophobic inhibitors from root exudates. *Biol Fertil Soils*, **58**(3): 251–264.

Rea P A. 2007. Plant ATP-binding cassette transporters. *Annu Rev Plant Biol*, **58**: 347–375.

Reiser S, Somerville C. 1997. Isolation of mutants of *Acinetobacter calcoaceticus* deficient in wax ester synthesis and complementation of one mutation with a gene encoding a fatty acyl coenzyme A reductase. *J Bacteriol*, **179**(9): 2969–2975.

Ryan P R, Tyerman S D, Sasaki T, Furuichi T, Yamamoto Y, Zhang W H, Delhaize E. 2011. The identification of aluminium-resistance genes provides opportunities for enhancing crop production on acid soils. *J Exp Bot*, **62**(1): 9–20.

Shen H, He L F, Sasaki T, Yamamoto Y, Zheng S J, Ligaba A, Yan X L, Ahn S J, Yamaguchi M, Sasakawa H, Matsumoto H. 2005. Citrate secretion coupled with the modulation of soybean root tip under aluminum stress. Up-regulation of transcription, translation, and threonine-oriented phosphorylation of plasma membrane H^+-ATPase. *Plant Physiol*, **138**(1): 287–296.

Sivaguru M, Liu J P, Kochian L V. 2013. Targeted expression of SbMATE in the root distal transition zone is responsible for sorghum aluminum resistance. *Plant J*, **76**(2): 297–307.

Souza E F C, Rosen C J, Venterea R T. 2021. Co-application of DMPSA and NBPT with urea mitigates both nitrous oxide emissions and nitrate leaching during irrigated potato production. *Environ Pollut*, **284**: 117124.

Steen E J, Kang Y S, Bokinsky G, Hu Z H, Schirmer A, McClure A, Del Cardayre S B, Keasling J D. 2010. Microbial production of fatty-acid-derived fuels and chemicals from plant biomass. *Nature*, **463**: 559–562.

Streubel J, Pesce C, Hutin M, Koebnik R, Boch J, Szurek B. 2013. Five phylogenetically close rice *SWEET* genes confer TAL effector-mediated susceptibility to *Xanthomonas oryzae* pv. *oryzae*. *New Phytol*, **200**(3): 808–819.

Subbarao G V, Ito O, Sahrawat K L, Berry W L, Nakahara K, Ishikawa T, Watanabe T, Suenaga K, Rondon M, Rao I M. 2006. Scope and strategies for regulation of nitrification in agricultural systems: Challenges and opportunities. *Crit Rev Plant Sci*, **25**(4):

303–335.

Subbarao G V, Tomohiro B, Masahiro K, Osamu I, Samejima H, Wang H Y, Pearse S J, Gopalakrishnan S, Nakahara K, Zakir Hossain A K M, Tsujimoto H, Berry W L. 2007. Can biological nitrification inhibition (BNI) genes from perennial *Leymus racemosus* (*Triticeae*) combat nitrification in wheat farming? *Plant Soil*, **299**(1): 55–64.

Subbarao G V, Nakahara K, Ishikawa T, Yoshihashi T, Ito O, Ono H, Ohnishi-Kameyama M, Yoshida M, Kawano N, Berry W L. 2008. Free fatty acids from the pasture grass *Brachiaria humidicola* and one of their methyl esters as inhibitors of nitrification. *Plant Soil*, **313**(1): 89–99.

Subbarao G V, Nakahara K, Hurtado M P, Ono H, Moreta D E, Salcedo A F, Yoshihashi A T, Ishikawa T, Ishitani M, Ohnishi-Kameyama M, Yoshida M, Rondon M, Rao I M, Lascano C E, Berry W L, Ito O. 2009. Evidence for biological nitrification inhibition in *Brachiaria* pastures. *Proc Natl Acad Sci USA*, **106**: 17302–17307.

Subbarao G V, Nakahara K, Ishikawa T, Ono H, Yoshida M, Yoshihashi T, Zhu Y Y, Zakir H A K M, Deshpande S P, Hash C T, Sahrawat K L. 2013a. Biological nitrification inhibition (BNI) activity in sorghum and its characterization. *Plant Soil*, **366**(1): 243–259.

Subbarao G V, Rao I M, Nakahara K, Sahrawat K L, Ando Y, Kawashima T. 2013b. Potential for biological nitrification inhibition to reduce nitrification and N_2O emissions in pasture crop-livestock systems. *Animal*, **7**: 322–332.

Subbarao G V, Sahrawat K L, Nakahara K, Rao I M, Ishitani M, Hash C T, Kishii M, Bonnett D G, Berry W L, Lata J C. 2013c. A paradigm shift towards low-nitrifying production systems: The role of biological nitrification inhibition (BNI). *Ann Bot*, **112**(2): 297–316.

Subbarao G V, Yoshihashi T, Worthington M, Nakahara K, Ando Y, Sahrawat K L, Rao I M, Lata J C, Kishii M, Braun H J. 2015. Suppression of soil nitrification by plants. *Plant Sci*, **233**: 155–164.

Subbarao G V, Kishii M, Bozal-Leorri A, Ortiz-Monasterio I, Gao X, Ibba M I, Karwat H, Gonzalez-Moro M B, Gonzalez-Murua C, Yoshihashi T, Tobita S, Kommerell V, Braun H J, Iwanaga M. 2021. Enlisting wild grass genes to combat nitrification in wheat farming: A nature-based solution. *Proc Natl Acad Sci USA*, **118**(35): e2106595118.

Sun L, Lu Y F, Yu F W, Kronzucker H J, Shi W M. 2016. Biological nitrification inhibition by rice root exudates and its relationship with nitrogen-use efficiency. *New Phytol*, **212**(3): 646–656.

Sun L, Di D W, Li G J, Kronzucker H J, Shi W M. 2017. Spatio-temporal dynamics in global rice gene expression (*Oryza sativa* L.) in response to high ammonium stress. *J Plant Physiol*, **212**: 94–104.

Sun L, Di D W, Li G J, Li Y L, Kronzucker H J, Shi W M. 2020. Transcriptome analysis of rice (*Oryza sativa* L.) in response to ammonium resupply reveals the involvement of phytohormone signaling and the transcription factor OsJAZ9 in reprogramming of nitrogen uptake and metabolism. *J Plant Physiol*, **246**/**247**: 153137.

Vioque J, Kolattukudy P E. 1997. Resolution and purification of an aldehyde-generating and an alcohol-generating fatty acyl-CoA reductase from pea leaves (*Pisum sativum*L.). *Arch Biochem Biophys*, **340**(1): 64–72.

Wang M, Qiao J Y, Yu C L, Chen H, Sun C D, Huang L Z, Li C Y, Geisler M, Qian Q, Jiang D A, Qi Y H. 2019. The auxin influx carrier, OsAUX3, regulates rice root development and responses to aluminium stress. *Plant Cell Environ*, **42**(4): 1125–1138.

Wang R, Ren C X, Dong S, Chen C, Xian B, Wu Q H, Wang J, Pei J, Chen J. 2021. Integrated metabolomics and transcriptome analysis of flavonoid biosynthesis in safflower (*Carthamus tinctorius* L.) with different colors. *Front Plant Sci*, **12**: 712038.

Wang X, Bai J H, Wang C, Xie T, Wang W, Wang D W, Zhang G L. 2023. Two newly-identified biological nitrification inhibitors in *Suaeda salsa*: Synthetic pathways and influencing mechanisms. *Chem Eng J*, **454**: 140172.

Weston L A, Ryan P R, Watt M. 2012. Mechanisms for cellular transport and release of allelochemicals from plant roots into the rhizosphere. *J Exp Bot*, **63**(9): 3445–3454.

Woodward E E, Hladik M L, Kolpin D W. 2016. Nitrapyrin in streams: The first study documenting off-field transport of a nitrogen stabilizer compound. *Environ Sci Technol Lett*, **3**(11): 387–392.

Ye R G, Wu Y R, Gao Z Y, Chen H, Jia L X, Li D M, Li X G, Qian Q, Qi Y H. 2021. Primary root and root hair development regulation by *OsAUX4* and its participation in the phosphate starvation response. *J Integr Plant Biol*, **63**(8): 1555–1567.

Yu C L, Sun C D, Shen C J, Wang S K, Liu F, Liu Y, Chen Y L, Li C Y, Qian Q, Aryal B, Geisler M, Jiang D A, Qi Y H. 2015. The auxin transporter, OsAUX1, is involved in primary root and root hair elongation and in Cd stress responses in rice (*Oryza sativa* L.). *Plant J*, **83**(5): 818–830.

Zakir H A K M, Subbarao G V, Pearse S J, Gopalakrishnan S, Ito O, Ishikawa T, Kawano N, Nakahara K, Yoshihashi T, Ono H, Yoshida M. 2008. Detection, isolation and characterization of a root-exuded compound, methyl 3-(4-hydroxyphenyl) propionate, responsible for biological nitrification inhibition by *Sorghum* (*Sorghum bicolor*). *New Phytol*, **180**(2): 442–451.

Zeng H Q, Di T J, Zhu Y Y, Subbarao G V. 2016. Transcriptional response of plasma membrane H^+-ATPase genes to ammonium nutrition and its functional link to the release of biological nitrification inhibitors from sorghum roots. *Plant Soil*, **398**(1): 301–312.

Zhang M, Fan C H, Li Q L, Li B, Zhu Y Y, Xiong Z Q. 2015. A 2-yr field assessment of the effects of chemical and biological nitrification inhibitors on nitrous oxide emissions and nitrogen use efficiency in an intensively managed vegetable cropping system. *Agric Ecosyst Environ*, **201**: 43–50.

Zhang M X, Zeng H Q, Afzal M R, Gao X, Li Y X, Subbarao G V, Zhu Y Y. 2022. BNI-release mechanisms in plant root systems: Current status of understanding. *Biol Fertil Soils*, **58**(3): 225–233.

Zhang X N, Lu Y F, Yang T, Kronzucker H J, Shi W M. 2019. Factors influencing the release of the biological nitrification inhibitor 1, 9-decanediol from rice (*Oryza sativa* L.) roots. *Plant*

Soil, **436**(1–2): 253–265.

Zhang Y T, Yang L W, Yang J J, Hu H L, Wei G Q, Cui J B, Xu J. 2022. Transcriptome and metabolome analyses reveal differences in terpenoid and flavonoid biosynthesis in *Cryptomeria fortunei* needles across different seasons. *Front Plant Sci*, **13**: 862746.

Zhao H M, Ma T F, Wang X, Deng Y T, Ma H L, Zhang R S, Zhao J. 2015. OsAUX1 controls lateral root initiation in rice (*Oryza sativa* L.). *Plant Cell Environ*, **38**(11): 2208–2222.

Zhao J, Dixon R A. 2009. MATE transporters facilitate vacuolar uptake of epicatechin 3′-*O*-glucoside for proanthocyanidin biosynthesis in *Medicago truncatula* and *Arabidopsis*. *Plant Cell*, **21**(8): 2323–2340.

Zheng Y N, Li L L, Liu Q, Yang J M, Wang X W, Liu W, Xu X, Liu H, Zhao G, Xian M. 2012. Optimization of fatty alcohol biosynthesis pathway for selectively enhanced production of C12/14 and C16/18 fatty alcohols in engineered *Escherichia coli*. *Microb Cell Fact*, **11**: 65.

(Managing Editor: WU Yawen)